Chapter 9
Model-Based Interpretations of Experimental Data Related to the Control of Balance During Stance and Gait in Humans

Robert J. Peterka

Abstract An important goal in developing a model is to explain experimental data from a physiological system in a manner that provides insight into the function of that system. We begin by using data from experiments that characterized the dynamic properties of the human balance control system that regulates body orientation during stance. The dynamic properties of stance control are expressed as frequency response functions derived from body sway evoked by pseudorandom stimuli that tilted the surface upon which subjects stood or the visual surround that they viewed. A feedback control model is developed in a step-wise manner in order to illustrate how different subsystems of the model combine to explain the features of the experimental data and to reveal (1) the contributions of feedback control based on sensory measures of body motion from proprioceptive, visual, and vestibular systems, (2) the regulation of the responsiveness to perturbations using sensory reweighting, (3) the contribution of positive torque feedback, and (4) the influence of passive dynamics of muscle/tendon systems. The insights obtained from this stance control model are then applied to aid in the interpretation of new results from experiments that investigate the control of body orientation during a gait-like task of stepping-in-place.

Keywords Modeling · Balance · Stance · Gait · Stepping · Sensory integration · Sensory reweighting · Human

9.1 Introduction

Our objectives in this chapter are (1) to demonstrate the steps involved in the development of a mathematical model that has sufficient complexity to provide insight into how the nervous system controls balance during quiet stance and (2) to illustrate how this model can provide insight into the mechanisms contributing to balance during gait.

R. J. Peterka (✉)
Department of Biomedical Engineering, Oregon Health & Science University,
3303 SW Bond Avenue, CH13B, Portland, OR 97239, USA
e-mail: peterkar@ohsu.edu

B. I. Prilutsky, D. H. Edwards (eds.), *Neuromechanical Modeling of Posture and Locomotion,* Springer Series in Computational Neuroscience,
DOI 10.1007/978-1-4939-3267-2_9

For the control of balance during quiet stance, it is well accepted that humans use orientation and motion information derived from sensory systems to generate corrective actions that resist the destabilizing effects of gravity, external perturbations, and internal perturbations in order to maintain a desired body orientation. These active, sensory-driven contributions to balance control act together with passive contributions that arise primarily from the intrinsic mechanical properties of muscle/tendon systems. The primary sensory systems contributing to balance control are the somatosensory/proprioceptive system (signaling forces applied to and within the body in addition to the orientation and motion of body segments relative to one another), visual system (signaling head orientation and motion relative to the visual environment), and vestibular system (signaling head orientation and motion in space) (Nashner 1981; Horak and Macpherson 1996).

In principle, the central nervous system could combine information from visual and vestibular sensors with multi-segmental proprioceptive cues in order to derive an estimate of body center-of-mass (CoM) orientation (Mergner 2004). Because of the importance of the concept of the CoM in describing and predicting the motion of mechanical systems in classical physics, it is common in discussions of balance control to assume that the nervous system can derive an estimate the body's CoM orientation from available sensory information and then generate corrective responses based on the deviation of the CoM from a desired position. We will use this assumption in the balance control model developed below because our goal is to lead the reader, who might not be familiar with physiological system modeling, through a logical progression of steps that illustrate how a model of balance control can be developed and how that development can enhance our understanding of the balance control system.

We will also make the assumption that the body mechanics are those of a single-segment inverted pendulum with body sway occurring about an ankle joint such that the ankle-joint angle also defines the CoM sway angle with respect to the stance surface. Because we are focusing on the development of a relatively simple model, we will not be considering studies that have used modeling to understand balance control in a more complex system that controls a multi-segmental body (van der Kooij et al. 1999; Park et al. 2004; Alexandrov et al. 2005; Fujisawa et al. 2005; Kiemel et al. 2008; Hettich et al. 2014; Kim et al. 2012; Li et al. 2012; Pasma et al. 2012; Boonstra et al. 2013).

In quasi-static conditions of quiet or mildly perturbed stance, physics dictates that stability is assured if motor actions can maintain body orientation such that the body CoM remains within the base of support defined by the area under and between the feet. Therefore, the task of balance control during stance is mainly a task of controlling body orientation. However, in the dynamic conditions that occur during a typical walking gait, there are periods in the gait cycle when the CoM is not within the base of support (Winter 1995). In these dynamic conditions, stability requires that natural body dynamics and/or motor actions constrain the CoM motion to follow a nominal, repeating trajectory and to return to that trajectory following a perturbation. Theoretical and experimental studies of dynamic stability during gait have been concerned mainly with characterizing the repeatability of trajectories

during the gait cycle (Dingwell and Cusumano 2000; Terry et al. 2012; Mummolo et al. 2013) and with investigating mechanisms that influence gait variability (Bauby and Kuo 2000; Dean et al. 2007; Ahn and Hogan 2013). Less well investigated are the mechanisms that regulate body orientation during gait.

In this chapter we will develop and apply a model that gives insights into how humans control body orientation during stance and gait. We will first describe the methods used to obtain an extensive experimental data set that has sufficient complexity to guide and constrain the development of a model for the control of body orientation during stance. We will develop this stance control model in stages so that the reader can clearly see that different components of the model account for different features of the experimental data. Then the results from stance control experiments will be compared to results from similar experiments performed during gait. To interpret the results from gait experiments, knowledge gleaned from the model-based interpretation of stance data will be used to determine the extent to which balance mechanisms contributing to body orientation control during stance also contribute to body orientation control during gait.

9.2 An Experimental Data Set Worthy of Modeling

In order to develop a comprehensive model of the human stance control system, an extensive set of experimental data are required. If a data set is too limited then multiple models may be equally effective in accounting for the experimental data with no way to distinguish among them. A comprehensive data set provides the constraints necessary to capture functionally important characteristics of the control system and distinguishing between different models.

In our studies of balance control we have extensively used a particular type of pseudorandom stimulus. Specifically, our pseudorandom stimulus is derived from a "maximal length ternary sequence" of numbers (Davies 1970). The ternary sequence of 0's, 1's, and -1's are mapped into a set of velocity steps with amplitudes of 0, +v, and −v with each value in the sequence having a step duration of Δt seconds. This velocity waveform has the property of a white noise stimulus where the amplitude spectrum of the stimulus is approximately constant out to a bandwidth of about 1/3Δt Hz. The velocity waveform is integrated to give a stimulus position waveform that we have used as stimuli to control, for example, the angular position of the support surface that subjects stand on or the visual surround that subjects view (Peterka 2002; Goodworth and Peterka 2010b).

Figure 9.1a shows an example of one complete cycle of a pseudorandom stimulus waveform (2° peak-to-peak amplitude) based on a maximal length ternary sequence and the corresponding evoked CoM body sway (averaged across five cycles). Data are from a subject with normal sensory function standing with eyes closed on the rotating surface. The subject's ankle joints were aligned with the rotation axis of the surface such that surface rotations evoked body sway in the sagittal plane.

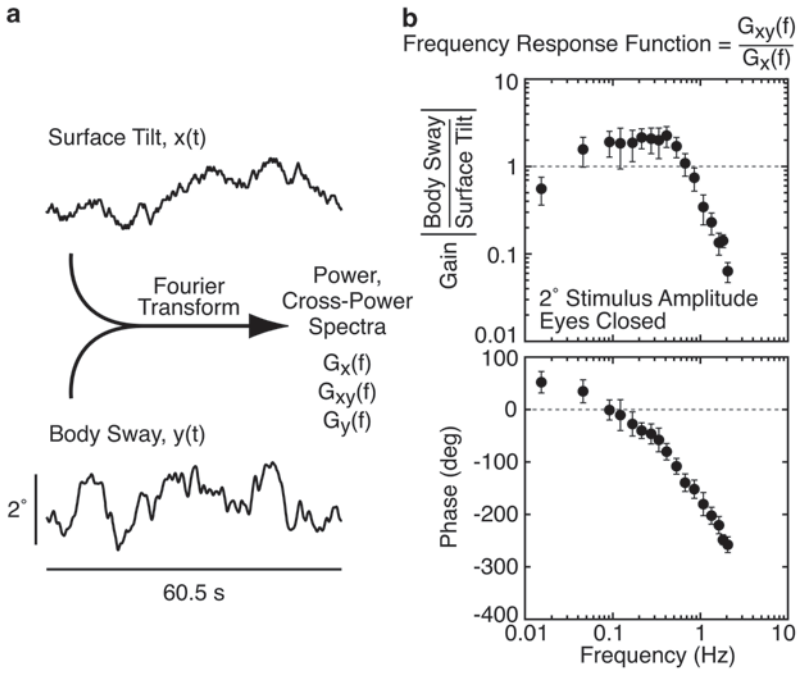

Fig. 9.1 Method to determine dynamic characteristics of the human balance control system during stance using wide-bandwidth pseudorandom stimulation. **a** A subject's balance was perturbed using pseudorandom stimuli that evoked a sagittal plane body sway response consisting of an angular tilt of the subject's center-of-mass from a vertical orientation. One cycle of a pseudorandom stimulus is shown (*top* trace; peak-to-peak amplitude of 2°). The stimulus controlled the angular tilt of the surface upon which the subject stood with eyes closed. The average body sway response (*bottom* trace; averaged across five cycles) is shown. Discrete Fourier transforms were applied to the stimulus and response data, and the transformed data were used to calculate power spectra of the stimulus and response, and the cross-power spectrum between the stimulus and response. **b** The ratio of the cross-power spectrum to the stimulus power spectrum provides an estimate of the frequency response function that defines the dynamic characteristics of the balance control system. The frequency response function can be expressed as gain and phase functions that describe the relative amplitude and timing, respectively, of body sway evoked by the stimulus across a range of stimulus frequencies. Error bars show 95% confidence intervals calculated following the procedures defined in Otnes and Enochson (1972).

We applied a standard frequency-domain analysis (defined in Otnes and Enochson (1972). Bendat and Piersol 2000; Pintelon and Schoukens 2012) using a discrete Fourier transform of the stimulus and CoM response waveforms to break down the time-domain waveforms into an equivalent set of sinusoidal components ranging from a frequency of 1/(cycle duration) = 0.0165 Hz in this example to an upper frequency of about 2 Hz. Results from the discrete Fourier transforms are used to calculate the power spectra of the stimulus and response, and the cross-power spectrum between stimulus and response for each stimulus cycle. The spectra are smoothed by averaging power spectra across the stimulus cycles and across selected ranges of frequency components in order to reduce variability.

The ratio of the cross power spectrum between stimulus and response to the stimulus power spectrum provides an estimate of the frequency response function (FRF). An FRF can be expressed as gain and phase functions, as shown in Fig. 9.1b, with the gain values indicating the ratio of CoM response amplitude to stimulus amplitude and the phase indicating the timing of the response relative to the stimulus. For a linear system, the FRF provides full knowledge of the system dynamics such that the response to any arbitrary stimulus can be predicted (Pintelon and Schoukens 2012).

Although body sway responses to a stimulus at any particular amplitude showed no evidence for strong nonlinearities, it was evident, from results of an earlier study using sinusoidal stimuli of varying amplitudes, that the response gain was not constant across all stimulus amplitudes (as expected for a linear system), but gain decreased with increasing amplitude (Peterka and Benolken 1995). Therefore, when we performed experiments using pseudorandom stimuli (Peterka 2002; Cenciarini and Peterka 2006; Goodworth and Peterka 2009, 2010a, b), a range of amplitudes was applied in each of the various test conditions. For example in our first study using pseudorandom stimuli (Peterka 2002) we applied stimuli with peak-to-peak amplitudes of 0.5°, 1°, 2°, 4°, and 8° in each of six test conditions. Examples of the family of FRFs for two of the test conditions, one for a surface stimulus with eyes closed and the other a visual stimulus during stance on a fixed and level surface, are shown in Fig. 9.2a and b, respectively.

The general shapes of the gain and phase data of all FRFs were quite similar across amplitude for both surface and visual stimuli. For each FRF, the gain was largest in the mid-frequency region of ~0.1–1 Hz and decreased with both decreasing and increasing frequency. The phase data showed phase leads at the lowest frequencies, increasing phase lags with increasing frequency, and a zero crossing at about 0.2 Hz. Although the general FRF shapes were similar for both surface and visual stimuli, there were some notable differences. For surface-tilt stimuli, the FRF gains from the various stimulus amplitudes tended to converge at about 1 Hz while this did not occur for FRF gains from the visual stimulus. The higher frequency phases from different stimulus amplitudes tended to diverge for surface-tilt stimuli with the phase from higher amplitude stimuli showing less phase lag. In contrast, the higher frequency phases from visual stimuli showed no change with stimulus amplitude.

The FRFs in Fig. 9.2a and b provide a representative data set that guides the model development described in the next section.

9.3 Development of a Stance Control Model

In the following subsections we will demonstrate the step-by-step development of a model that accounts for a wide variety of experimental FRF results. The stages of model development, from simple to more complex, correspond quite well with the thought processes that were applied in the original model development.

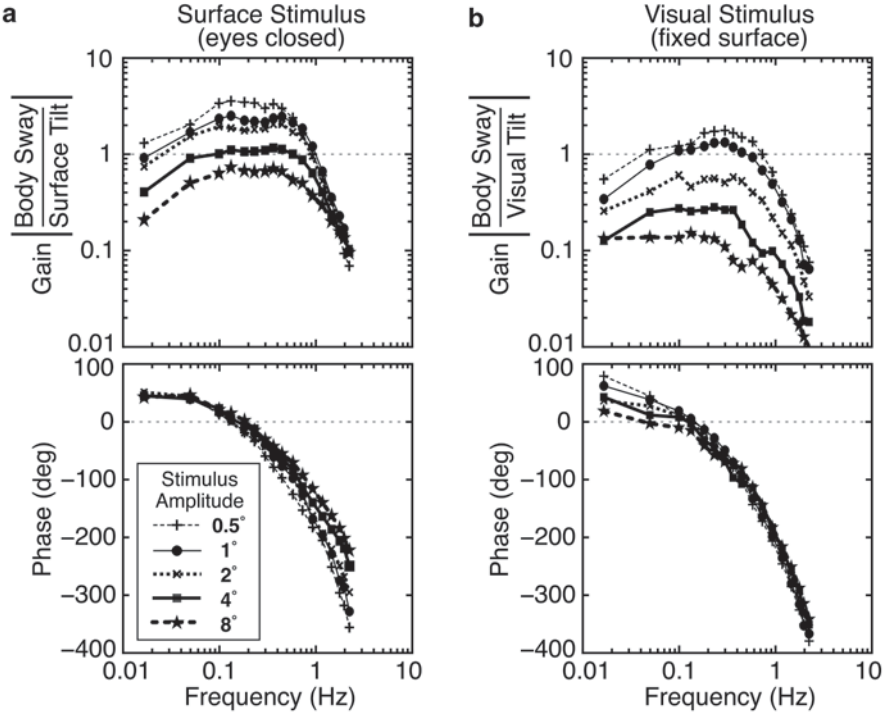

Fig. 9.2 Sets of frequency response functions calculated using pseudorandom stimuli with five different amplitudes. Stimuli were either (**a**) support surface tilts during eyes closed stance or (**b**) visual surround tilts during stance on a fixed and level surface. (Data plots abstracted from Peterka (2002))

9.3.1 Basic Feedback Control Model of Stance

It is widely recognized that balance control is organized as a feedback control system with the feedback provided by body orientation information obtained from sensory systems (Johansson et al. 1988; Horak and Macpherson 1996). Figure 9.3a shows a block diagram of a simple model that is capable of partially describing experimental FRFs and that includes the basic system components that we can reasonably assume to be present in the system. These include the body mechanics, a sensory system that detects body sway, a "neural controller" that converts the detected body sway into a corrective torque, T_c, applied about the ankle joints, and a time delay element representing all the delays in the system (i.e., sensory transduction, transmission of sensory information, processing of sensory and motor control information, transmission of motor control signals, and muscle activation delays).

The body mechanics are that of a single-segment inverted pendulum. The equation of motion for the inverted pendulum is:

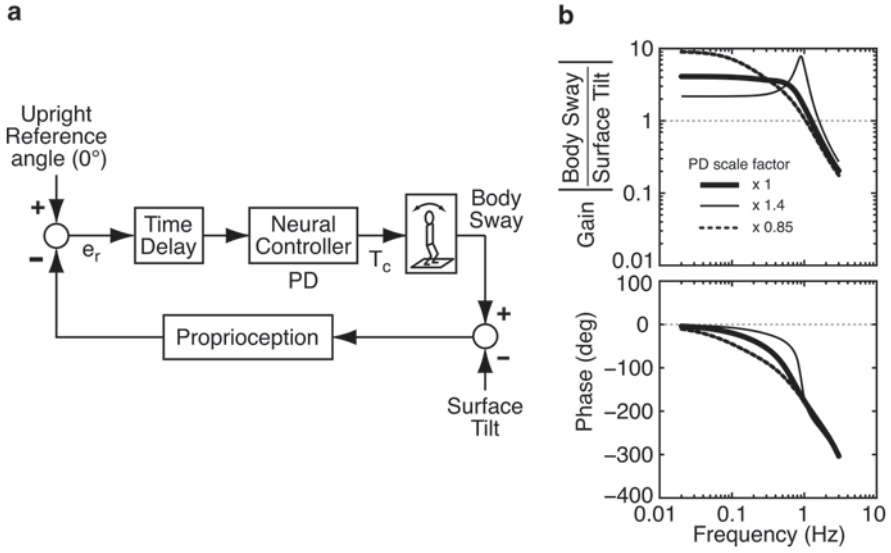

Fig. 9.3 Simple feedback control model of the balance control system (**a**) and model predictions expressed in the form of frequency response functions (**b**). Model assumes a one-segment inverted pendulum body is controlled by sensory feedback from proprioception signaling body sway angle relative to the surface. The frequency response functions show the effect of changing the values of the PD parameters (that define proportional and derivative feedback gains) on the dynamic characteristics of the system. The "x 1" PD scale factor uses PD parameter values defined in Table 9.2 and produces gain and phase functions that most closely resemble experimental data. The body inverted pendulum parameters are given in Table 9.1

$$J\frac{d^2\theta_{bs}(t)}{dt^2} = mgh \cdot sin(\theta_{bs}(t)) + T_c(t) \tag{9.1}$$

where $\theta_{bs}(t)$ is the time course of body-in-space sway angle (i.e., body sway with respect to earth vertical), J is the moment of inertia of the body about the ankle-joint axis, m is body mass (not including mass of the feet), h is height of the body CoM above the ankle joint, g is the gravitational constant, and $T_c(t)$ is a torque applied at the ankle joint. This time-domain equation can be linearized for small angles of motion (i.e., $\theta_{bs}(t) \cong \sin(\theta_{bs}(t))$) and expressed in the Laplace domain:

$$\frac{\theta_{bs}(s)}{T_c(s)} = \frac{1}{Js^2 - mgh} \tag{9.2}$$

where s is the Laplace variable. The Laplace representation is useful because (1) it allows for the algebraic manipulation of the differential equations that describe the input-output relations of each model component (i.e., each block in the block diagram) and (2) it allows for the calculation of FRFs by substitution of $s = j2\pi f$ with j being the imaginary number $\sqrt{-1}$ and f being frequency in Hz.

The sensory system provides information about body sway. In the Fig. 9.3a model we consider that only proprioception is available and that proprioception signals body orientation relative to the surface (i.e., it encodes the ankle-joint angle). We also assume that the proprioceptive sensory signal is a perfect encoder of the ankle joint angle such that there are no sensory dynamics involved. Specifically, the "Proprioception" block in Fig. 9.3a is set to a value of "1" to represent this perfect encoding with no dynamics. Effectively, we are assuming that the spinal and central nervous systems are capable of deriving an essentially perfect encoding of limb motion by processing the complex afferent signals available from the peripheral sensors such as stretch receptors. Justification for this assumption comes from recordings from the cerebellum and the dorsal spinocerebellar tract where the neural signals do not show responses typical of stretch receptors, but rather show activity representing kinematic variables of limb motion (Bosco et al. 2000; Casabona et al. 2004).

The sensory-derived body orientation is compared to an internal reference indicating the desire to remain in an upright orientation. Any deviation from the reference produces and error signal $e_r(t) = \theta_{ss}(t) - \theta_{bs}(t)$ where $\theta_{ss}(t)$ is the tilt angle of the support surface. The time delayed error signal, $e_r(t - t_d)$ where t_d is length of the delay, is the input to the neural controller. The neural controller then generates a corrective torque in relation to the time-delayed error signal according to the time-domain equation:

$$T_c(t) = K_p \bullet e_r(t - t_d) + K_d \bullet \frac{de_r(t - t_d)}{dt} \qquad (9.3)$$

The Laplace domain version is:

$$\frac{T_c(s)}{e_r(s)} = (K_p + K_d \bullet s) \bullet e^{-t_d s} \qquad (9.4)$$

where K_p is the proportionality constant for the error angular position and K_d is the proportionality constant for the error angular velocity. In engineering systems this type of controller is referred to as a PD (proportional-derivative) controller. With all the components of the model now defined we can write an equation in the Laplace domain and then solve for the ratio of the body sway response to the surface-tilt stimulus:

$$\theta_{bs}(s) = \frac{T_c(s)}{e_r(s)} \cdot \frac{\theta_{bs}(s)}{T_c(s)} \cdot e_r(s) = \frac{(K_p + K_d s) \cdot e^{-t_d s}}{Js^2 - mgh} (\theta_{ss}(s) - \theta_{bs}(s)) \qquad (9.5)$$

$$\frac{\theta_{bs}(s)}{\theta_{ss}(s)} = \frac{(K_p + K_d s) \bullet e^{-t_d s}}{Js^2 - mgh + (K_p + K_d s) \bullet e^{-t_d s}} \qquad (9.6)$$

Table 9.1. Model parameters for inverted pendulum body mechanics

Parameter	Description	Value
J	Moment of inertia about ankle joint	81 kg m^2
m	Body mass (not including feet)	83 kg
h	Center-of-mass height above ankle joint	0.9 m
mgh	Gravity torque constant	733 kg m^2/s^2

Table 9.2 Model parameters for feedback control

Parameter	Description	Value
K_p	Neural controller proportional (P) gain constant	968 (1060) Nm/rad
K_d	Neural controller derivative (D) gain constant	350 (286) Nms/rad
K_t	Torque feedback gain constant	8.7×10^{-4} rad/Nm
τ_t	Torque feedback low-pass filter time constant	15 s
t_d	Time delay	0.18 s

K_p and K_d values in parentheses were used in the model shown in Fig. 9.6a that included stretch reflex and Hill muscle/tendon subsystem

After making the $s = j2\pi f$ substitution, FRF values expressed as real and imaginary numbers at each frequency, f, can be calculated and then represented as gain and phase values by:

$$\text{FRF gain} = \left| \frac{\theta_{bs}(j2\pi f)}{\theta_{ss}(j2\pi f)} \right| = \sqrt{Re(\bullet)^2 + Im(\bullet)^2} \tag{9.7}$$

$$\text{FRF phase} = \frac{180^\circ}{\pi} \bullet \text{atan}(Im(\bullet) / Re(\bullet)) \tag{9.8}$$

where $Re(\cdot)$ and $Im(\cdot)$ refer to the real and imaginary components, respectively, of the FRF values and phase is expressed in degrees.

Assuming fixed values for the J, m, and h parameters for a give subject (see Table 9.1), the shapes of the gain and phase curves depend on the particular values of the parameters K_p, K_d, and t_d (see Table 9.2). The rather large time delay value (0.18 s) accounts for a portion of the large and increasing phase lags seen at higher frequencies (consistent with experimental FRF phases). Three different gain and phase curves are shown in Fig. 9.3b to demonstrate the effect of varying K_p and K_d values. The curves labeled as having PD controller values scaled by a "x 1" scale factor result in FRF gain and phase curves that are closest to the shape of experimental FRFs shown in Fig. 9.2.

Consistent with most experimental FRF gains shown in Fig. 9.2, the FRF gains at low to mid-frequencies are greater than unity for all FRFs shown in Fig. 9.3b. These low-frequency gain values calculated for the Fig. 9.3a model are determined by the value of K_p in relation to the value of the product mgh. Specifically, the low frequency gain is given by $K_p/(K_p - mgh)$ and this value is obviously always greater

than one. The value *mgh* is a scale factor that specifies the amount of destabilizing torque due to gravity created per unit of body sway away from the upright orientation. The value of K_p must be greater than *mgh* in order that enough corrective torque is generated by the neural controller to resist the destabilizing torque due to gravity. For the FRF shown in Fig. 9.3b that most closely resembles the shape of the experimental FRFs (the times one PD scale factor), the low frequency gain is approximately equal to 4 and thus K_p has a value that is about 1/3rd greater than *mgh*.

This relatively low value of K_p makes this simple control system quite sensitive to even small perturbations caused by a non-level support surface. With this simple feedback model, the only way to reduce the sensitivity to surface tilt would be to increase the value of K_p. However, increasing K_p produces an FRF with a resonant peak at ~1 Hz. (Fig. 9.3b shows the results of increasing both K_p and K_d but similar results are seen when only K_p is increased.) This necessitates a careful regulation of the neural controller PD values in order to avoid resonant behavior or even unstable operation. Furthermore, larger time delay values make the system shown in Fig. 9.3a more difficult to stabilize such that no PD values can be found that provide stability if the time delay is greater than about 0.35 s (van der Kooij and Peterka 2011).

In summary, the very simple model in Fig. 9.3a is successful in predicting the basic shape seen in experimental FRFs, but this model is clearly incomplete. The model cannot account for the stimulus amplitude-dependent variation in overall FRF gain magnitude while shapes of the FRF gain and the phase curves remain relatively unaffected. In this simple model, the gain can only be influenced by changes in controller parameters, but these changes also change the shapes of the gain and phase curves. The next subsection modifies the basic Fig. 9.3a model in order to account for stimulus-dependent gain changes.

9.3.2 Accounting for Stimulus Amplitude-Dependent FRF Gain

The addition to the Fig. 9.3a model that accounts for amplitude-dependent changes in overall FRF gain values is shown in Fig. 9.4a. This model is expanded to include feedback from visual and vestibular systems in addition to proprioception. The model includes a "sensory integration" subsystem that represents the process by which the orientation information from the three sensory systems is combined, by a weighted summation, to form an internal estimate of body orientation. This internal estimate is compared to an internal reference of the desired upright body orientation (as in the Fig. 9.3a model but not shown in Fig. 9.4a) with the difference between the estimate and the reference forming an orientation error signal, $e_r(t)$. This error signal is the input to the neural controller that produces the corrective torque.

The three sensory-system weights represent the relative contributions of the sensory systems to the overall internal estimate of body orientation. Mathematically this means that, for a given test condition, the sum of the weights of all sensory systems contributing to balance control is equal to unity. As in the Fig. 9.3a model,

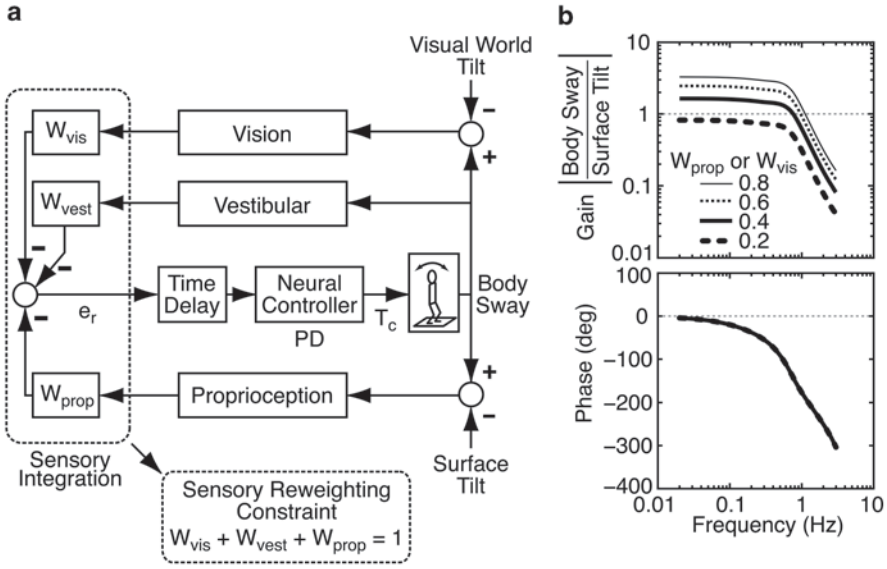

Fig. 9.4 A feedback control model that includes sensory integration (**a**) and model predictions expressed in the form of frequency response functions (**b**). The model predictions demonstrate how changes in the proprioceptive weight (for surface-tilt stimulation) or in visual weight (for visual-tilt stimuli) affect the frequency response functions. The body mechanics parameters and feedback control parameters are defined in Tables 9.1 and 9.2, respectively

we continue to assume that ankle proprioception provides a perfect sensory signal encoding the ankle joint angle and therefore the block labeled "Proprioception" has a value of "1". We make the same assumption for the "Vision" and "Vestibular" blocks.

For the vestibular system the justification for the assumption of perfect encoding of head tilt with respect to earth vertical comes from experimental studies that show evidence that central processing of sensory signals from the semicircular canals (encoding angular head velocity) and otolith organs (encoding an ambiguous combination of head linear acceleration and acceleration due to gravity) can separate the transient component of linear acceleration from the component of linear acceleration due to gravity (Angelaki et al. 1999; Merfeld et al. 1999; Zupan et al. 2000; Angelaki et al. 2004; Peterka et al. 2004). For our purposes the conclusion is that nervous system has available to it an accurate, wide-bandwidth estimate of the orientation of the gravity vector with respect to the head and therefore a vestibular-derived estimate of body orientation with respect to earth vertical.

For the visual system, justification for the presence of wide bandwidth encoding of visual motion information comes from experiments showing that (1) eye movements in humans evoked by optokinetic stimuli have approximately constant FRF gains over a wide bandwidth (Peterka et al. 1990) and (2) neural recordings from Purkinje cells in the cerebellar flocculus of Java monkeys have high sensitivity to optokinetic stimuli out to 3 Hz (Markert et al. 1988).

The Laplace equation for the Fig. 9.4a model when a surface-tilt stimulus is applied is:

$$\frac{\theta_{bs}(s)}{\theta_{ss}(s)} = \frac{W_{prop} \bullet (K_p + K_d s) \bullet e^{-t_d s}}{Js^2 - mgh + (K_p + K_d s) \bullet e^{-t_d s}} \tag{9.9}$$

When a visual-tilt stimulus is applied the equation is:

$$\frac{\theta_{bs}(s)}{\theta_{vs}(s)} = \frac{W_{vis} \bullet (K_p + K_d s) \bullet e^{-t_d s}}{Js^2 - mgh + (K_p + K_d s) \bullet e^{-t_d s}} \tag{9.10}$$

Both of these equations are derived with the assumption that the sum of the sensory weights is always unity. These two equations differ from Eq. (9.6) only by having an additional multiplying factor of either W_{prop} or W_{vis} in the numerator. Thus if the K_p, K_d, and t_d parameters of Eqs. (9.9) and (9.10) are set to the same values as used to calculate the FRFs shown in Fig. 9.3b, the FRF gain and phase curves will have the same shape as those shown in Fig. 9.3b. The only difference will be that the overall magnitude of the gain curves will depend on the value of W_{prop} for test conditions where a surface-tilt stimulus was applied and on the value of W_{vis} for conditions where a visual-tilt stimulus was applied.

The FRFs shown in Fig. 9.4b were calculated for 4 different W_{prop} or W_{vis} values ranging from 0.2 to 0.8 and with the remaining parameters set to values in Tables 9.1 and 9.2. The phase curves of the FRFs are not affected by changing W_{prop} or W_{vis} values, so the phase curves calculated for different sensory weights overlay one another in Fig. 9.4b. The gain curves calculated using Eqs. (9.9) and (9.10) are identical when W_{prop} and W_{vis} values are equal to one another. Changing the value of W_{prop} or W_{vis} simply shifts a gain curve up or down (when gain is plotted on a log-log scale).

The FRFs shown in Fig. 9.4b provide a better match to the experimental FRFs in Fig. 9.2 in that we now have an explanation that accounts for the decrease in FRF gains with increasing stimulus amplitude while the FRF phases are not affected by stimulus amplitude. Specifically, when applying a surface-tilt stimulus, the fact that the FRF gains are largest at the lowest stimulus amplitude and decrease with increasing stimulus amplitude implies that the proprioceptive contribution to balance control, quantified by W_{prop}, is greatest at the lowest stimulus amplitude and decreases with increasing amplitude. For eyes closed tests using surface-tilt stimuli, a decrease in W_{prop} with increasing stimulus amplitude also implies that the vestibular contribution to balance control (represented by W_{vest} in the model) increased with increasing stimulus amplitude. This increase in W_{vest} is implied because of the constraint that sensory weights must sum to unity.

The interpretation of experimental results based on the Fig. 9.4a model allows us to recognize the contribution of a “sensory reweighting phenomenon” to the regulation of balance. Specifically, an amplitude-dependent sensory reweighting

occurs such that the contribution to balance control from the sensory system encoding the primary perturbing stimulus (e.g., proprioception for surface movements) is decreased while the contribution from secondary sensory systems (e.g., the vestibular system in eyes closed tests) is increased. This model prediction of reciprocal reweighting has been tested and confirmed experimentally (Cenciarini and Peterka 2006).

However, the model-predicted FRFs in Fig. 9.4b are not yet entirely consistent with the experimental FRFs in Fig. 9.2. In particular, each of the experimental FRFs for both surface and visual stimuli show a decrease in gain and phase advance with decreasing frequency for frequencies below about 0.1 Hz. The next subsection will modify the Fig. 9.4a model to account for this low frequency behavior.

9.3.3 Accounting for Low Frequency FRF Gain Reduction and Phase Advance

If balance control were governed entirely by feedback control with the properties of the Fig. 9.4a model, the regulation of body orientation would be very sensitive to the static conditions in the environment. For example, the Fig. 9.4a model predicts that if a subject was relying 80% on proprioception for balance control and was standing on a surface that was tilted by only 1°, the subject's body would remain tilted from upright by almost 4°. That is, the Fig. 9.4a model predicts that equilibrium between the torque due to gravity and the corrective torque generated by the control system is achieved at a body angle of $W_{prop} \cdot K_p/(K_p - mgh)$ for a 1° surface-tilt angle. This equation shows that the only way to reduce the sensitivity to surface tilt would be to reduce W_{prop} (and therefore increase W_{vest} in this eyes-closed condition) or to greatly increase K_p. As shown in the Fig. 9.3b FRFs, it is not possible to greatly increase K_p. Furthermore, results based on optimal control concepts indicate that it is not desirable to rely heavily on vestibular information due to the high noise levels in the vestibular sensory system (van der Kooij and Peterka 2011). Therefore some other mechanism must be contributing to balance control to regulate low frequency or static body orientation.

An earlier sensory integration model attempted to account for the low frequency gain declines and phase advances by having a neural controller that includes integral control action in addition to PD control (i.e., PID control) (Peterka 2002). However, the PID controller did not fully account for the low frequency gain and phase data and motivated us to consider that the balance control system might exploit its ability to sense a sustained corrective torque in order to move the body toward a more upright orientation. The model originally proposed in Peterka (2002) was modified to include an additional feedback pathway based on sensory systems that encode the force exerted by muscle stretch and activation (e.g., by Golgi tendon organs) or by other somatosensory contributions such as sensing center-of-pressure (CoP) shifts on the feet (Peterka 2003; Cenciarini and Peterka 2006).

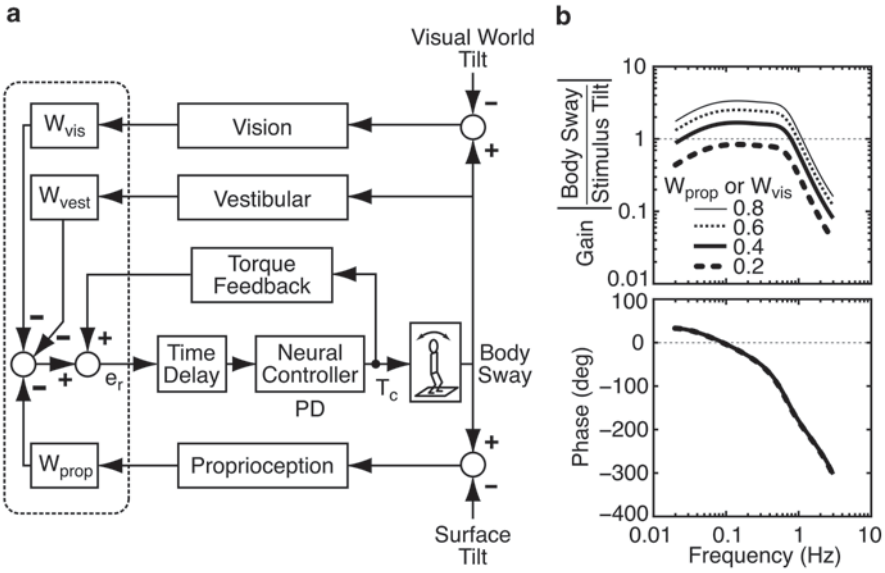

Fig. 9.5 A feedback control model that includes sensory integration and torque feedback (**a**) and model predictions expressed in the form of frequency response functions (**b**). The model predictions demonstrate how changes in the proprioceptive weight (for surface-tilt stimulation) or in visual weight (for visual-tilt stimuli) affect the frequency response functions. The torque feedback loop provides positive feedback such that the magnitude of corrective torque, T_c, is increased if T_c is sustained for longer periods of time. The increased T_c will move the body toward an upright position. The effect of the positive torque feedback is to reduce the low frequency gain and advance the low frequency phase of the frequency response functions. The body mechanics parameters and feedback control parameters are defined in Tables 9.1 and 9.2, respectively

A model that incorporates torque feedback is shown in Fig. 9.5a along with FRFs that demonstrate how the dynamic characteristics of the system are affected by inclusion of a torque feedback pathway. Note that the torque feedback pathway provides positive feedback. Positive force feedback has previously been understood to contribute to motor control in specific circumstances such as load compensation (Prochazka et al. 1997; Duysens et al. 2000). Functionally, the Fig. 9.5a model predicts that when a subject is leaning forward and generating a sustained corrective torque, the positive torque feedback causes the error signal to increase in value. The increased error signal generates additional corrective torque that overcomes the torque due to gravity such that the body is moved toward an upright position. As the body-sway angle decreases, the magnitude of corrective torque decreases, and the contribution of the positive torque feedback pathway diminishes.

To account for the experimental FRFs we found it necessary to include an integrator, or to be more physiologically realistic, a leaky integrator (i.e., a low-pass filter with a long time constant) in the torque feedback pathway. When torque feedback is included in the model, the equation describing the FRF becomes much more complicated and it is more informative to present it as follows:

$$\frac{\theta_{bs}(s)}{\theta_{ss}(s)} = \frac{W_{prop} \bullet B \bullet NC \bullet TD}{1 - TF \bullet NC \bullet TD + B \bullet NC \bullet TD} \tag{9.11}$$

where NC, B, TD, and TF are the Laplace equations for the neural controller, body mechanics, time delay, and torque feedback, respectively, given by $NC = K_p + K_d \bullet s, B = 1/(J \bullet s^2 - mgh)$, $TD = e^{-t_d s}$, and $TF = K_t / (\tau_t \bullet s + 1)$ The parameters K_t and τ_t are the gain and time constants, respectively, of the low-pass filter in the torque feedback pathway. As with the Fig. 9.4a model the assumption is that the sum of sensory weights is unity. The functional form of the FRF equation for a visual stimulus is the same except that W_{prop} in Eq. (9.11) is replaced with W_{vis}. As with the Fig. 9.4a model, variation in W_{prop} or W_{vis} produces FRF gain curves with different amplitudes but with identical shapes (when plotted on log-log axes) and the FRF phase curves are the same for all values of W_{prop} or W_{vis}. The model-predicted FRFs now show a gain decrease and phase advance at lower frequencies, consistent with the experimental FRFs shown in Fig. 9.2.

The FRFs predicted by the Fig. 9.5a model now closely resemble FRFs across the entire bandwidth of test frequencies from experiments using visual stimuli (Fig. 9.2b) but the resemblance is not quite as good for surface stimuli (Fig. 9.2a). Specifically, experimental FRFs obtained using different amplitudes of surface stimuli show a convergence of the gain curves in the 1–2 Hz region and a divergence of the phase curves with increasing frequency. The next subsection considers an extension of the Fig. 9.5a model that includes additional mechanisms.

9.3.4 *Accounting for FRF Differences for Surface and Visual Stimuli*

The differences between experimental FRFs from surface and visual stimuli occur mainly at higher frequencies. If a single model can account for both sets of FRFs then there must be some asymmetry in the balance control system that causes responses evoked by a surface-tilt stimuli to differ from those evoked by visual stimuli. There are two obvious oversights in the models considered so far. One is the absence of a contribution from passive muscle/tendon mechanics, and the second is the absence of a stretch reflex contribution to muscle activation.

The model shown in Fig. 9.6a adds these two components. The muscle/tendon properties were modeled using a linearized Hill-type model (McMahon 1984) that included an elastic element in series with a parallel combination of a contractile component (generating internal muscle force), and elastic and damping elements. Inclusion of this muscle/tendon system alters the balance control model in two ways. First, the passive mechanical properties of the muscle/tendon system generate an ankle torque, T_{pas}, as a function of ankle joint motion. This torque is generated without time delay. T_{pas} sums with the torque generated by active muscle contractions, T_{act}, to produce that total corrective ankle torque, T_c. Second, the activation of

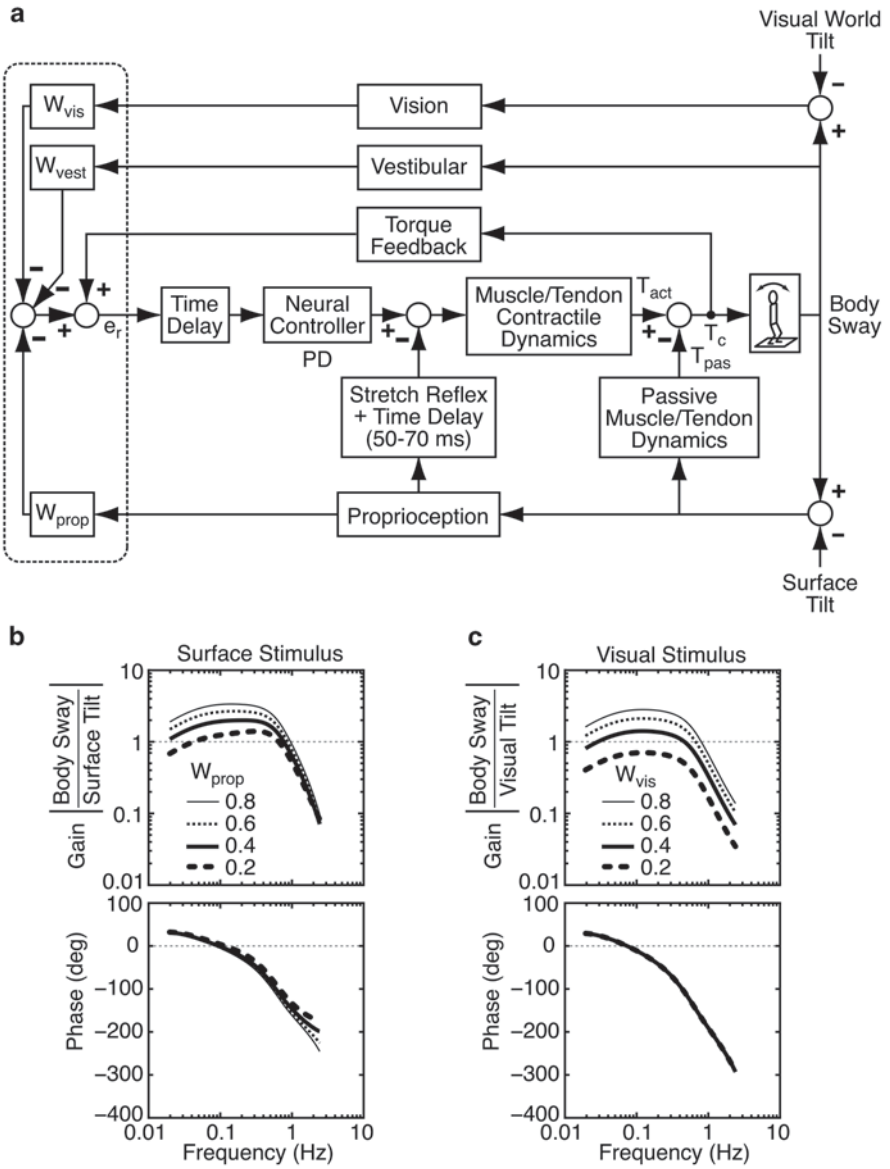

Fig. 9.6. A feedback control model that includes sensory integration, torque feedback, stretch reflex, muscle/tendon contractile dynamics, and passive muscle/tendon dynamics (**a**) and model predictions expressed in the form of frequency response functions (**b**, **c**). The stretch reflex is assumed to generate a muscle activation signal proportional to the velocity of ankle joint motion. The muscle/tendon contractile and passive dynamics are based on a linearized Hill-type muscle/tendon system. With the addition of stretch reflex and muscle/tendon components, the model-predicted frequency response functions for surface-tilt stimuli (**b**) and visual-tilt stimuli (**c**) now resemble experimental frequency response functions in Fig. 9.2. The body mechanics parameters, feedback control parameters, and stretch reflex and muscles/tendon parameters are defined in Tables 9.1, 9.2, and 9.3, respectively

the muscle contractile element generates an internal muscle force that acts through, and is effectively low-pass filtered by the muscle mechanics to produce T_{act}. The output of the neural controller is now considered to be a muscle activation signal, rather than an applied ankle torque.

The stretch reflex is represented as a subsystem whose output is a muscle activation signal that is a function of the angular velocity of the ankle joint motion. The stretch reflex output is summed with the activation signal from the neural controller. The stretch reflex includes a time delay that is assumed to be shorter than the delay associated with the sensory integration mechanism.

With the addition of muscle/tendon and stretch reflex components, the Laplace equations describing body sway responses to surface and visual stimuli now differ from one another. These equations are:

$$\frac{\theta_{bs}(s)}{\theta_{ss}(s)} = \frac{B \bullet (P + SR) + W_{prop} \bullet B \bullet NC \bullet M \bullet TD}{1 - TF \bullet NC \bullet M \bullet TD + B \bullet (P + SR) + B \bullet NC \bullet M \bullet TD} \tag{9.12}$$

$$\frac{\theta_{bs}(s)}{\theta_{vs}(s)} = \frac{W_{vis} \bullet B \bullet NC \bullet M \bullet TD}{1 - TF \bullet NC \bullet M \bullet TD + B \bullet (P + SR) + B \bullet NC \bullet M \bullet TD} \tag{9.13}$$

where M, P, and SR are the Laplace equations for linearized Hill-type muscle/tendon contractile dynamics, passive muscle/tendon dynamics, and stretch reflex dynamics, respectively. The Laplace equations for these components are $M = K_{se} / (K_{ce} + K_{se} + B_{ce} \cdot s)$, $P = (K_{se} \cdot K_{ce} + K_{se} \cdot B_{ce} \cdot s) / (K_{ce} + K_{se} + B_{ce} \cdot s)$, and $SR = B_{sr} \bullet s \bullet e^{-t_{sr} \cdot s}$. The additional model parameters (values given in Table 9.3 include the linearized Hill-type muscle/tendon properties of series elastic stiffness, K_{se}, contractile element stiffness, K_{ce}, and contractile element damping, B_{ce}. The functional stretch reflex is assumed to contribute a muscle activation signal proportional to ankle velocity (proportionality constant B_{sr}) and with time delay t_{sr}. Note that the passive muscle/tendon dynamics have properties of a "lead/lag" system that generates more passive torque for higher compared to lower frequencies of ankle joint motion. The muscle/tendon contractile dynamics have the functional form of a low-pass filter. The static gain of this filter is $K_{se}/(K_{se}+K_{ce})$, which is less than unity. Therefore adjustments in system parameters are necessary to make up for this gain reduction such that the overall dynamic characteristics of the balance control system remain similar to the ones shown for the Fig. 9.5a model. The adjusted parameter values are shown in parentheses in Table 9.2.

Table 9.3 Model parameters for stretch reflex and muscle/tendon subsystems

Parameter	Description	Value
B_{sr}	Stretch reflex velocity gain constant	115 Nms/rad
t_{sr}	Stretch reflex time delay	0.07 s
K_{se}	Hill muscle/tendon subsystem series element stiffness	660 Nm/rad
K_{ce}	Hill muscle/tendon subsystem contractile element stiffness	147 Nm/rad
B_{ce}	Hill muscle/tendon subsystem contractile element damping	22 Nms/rad

With a proper selection of parameters, Eqs. (9.12) and (9.13) now predict a set of FRFs that differ for surface and visual stimuli (Fig. 9.6b and c) and that display characteristics that approximately match those of experimental FRFs. The set of visual FRFs shown in Fig. 9.6c are very similar to the ones predicted by the Fig. 9.5a model that did not include the stretch reflex or muscle/tendon mechanics. This similarity occurs because a visual stimulus only indirectly evokes body sway causing ankle-joint motion. That is, the dynamics of the balance control system effectively filters out the higher frequency components of the visual stimulus leaving only lower frequency component of the ankle-joint motion. This limits the higher frequency, velocity-related contributions to corrective torque arising from the stretch reflex and passive muscle/tendon mechanics. In contrast, the same stimulus applied to the surface directly activates the stretch reflex and passive muscle/tendon pathways such that the higher frequency components of the stimulus contribute additional corrective torque at higher frequencies (as compared to the visual stimulus), thus affecting the higher frequency dynamics of the balance control system (Fig. 9.6b). Furthermore, as the surface-tilt amplitude increases, the proprioceptive weight, W_{prop}, decreases. With decreasing W_{prop} the influence of the stretch reflex contribution and passive muscle/tendon mechanics on overall response dynamics increases in comparison to the influence of the proprioceptive contribution from the sensory integration subsystem. Thus, the FRF gain curves from surface stimuli change in shape as well as magnitude, and the FRF phase curves change shape as W_{prop} changes.

9.3.5 Limitations and Extensions of the Stance Control Model

The predictions from the Fig. 9.6a model suggest that we can now account for the major features of experimental FRFs. It seems like it should be possible to obtain reliable measures of the various model parameters by applying optimal estimation methods to fit the model FRF equation to the experimental FRF data (see details of fitting methods in (Peterka 2002; van der Kooij and Peterka 2011)). Assuming that we use estimates of parameters associated with body mechanics (J, m, h) obtained from anthropometric measures, there are 11 additional free parameters in Eqs. (9.12) and (9.13).

Unfortunately, limitations in our ability to reliably identify the free parameters are quickly revealed from the results of optimal estimation procedures to determine model parameters. A major difficulty is that there is considerable redundancy in that, for some combinations of parameters, more than one parameter can account for particular features of the FRFs. To overcome this problem of parameter redundancy, our approach in previous studies (Peterka 2002, 2003; Cenciarini and Peterka 2006; van der Kooij and Peterka 2011) has been to simplify the model to reduce redundancies in parameters. The simplified model in these previous studies did not include the stretch reflex subsystem and muscle/tendon contractile dynamics subsystem, and the passive muscle/tendon dynamics were simplified by representing this subsystem as a summation of stiffness and damping elements (i.e., $P = K_{pas} + B_{pas} \cdot s$) rather than the more complex definition of P used in Eqs. (9.12) and (9.13). With these simplifications, the number of free parameters is reduced to

eight and the optimal fits to the experimental FRFs typically yield reliable parameters in the sense that the variance of parameters across subjects is relatively low. However, the tradeoff for this reduced variability is the recognition that the model is deviating from reality to some extent.

Another approach to enhancing our ability to identify parameters of more realistic models is to gather more complex data sets. More complex data sets could be obtained from experiments that include stimuli with wider bandwidths (Goodworth and Peterka 2009, 2010b, 2012), stimuli that include multiple types of perturbations that are presented simultaneously (e.g., combinations of visual-tilt stimuli, surface-tilt stimuli, surface translations, galvanic vestibular stimulation, and/or applications of external force; see (Cenciarini and Peterka 2006; Pasma et al. 2012; Boonstra et al. 2013)), and recordings of additional "in-the-feedback-loop" signals such as muscle activation signals recorded using electromyography (Kiemel et al. 2008) or muscle motion recorded using ultrasound techniques (Loram et al. 2005). The idea is that the added richness of the experimental data will provide sufficient additional information to allow for the reliable identification of more realistic models that include the added parameters that are necessary to represent the various subsystems contributing to balance control.

Since a particular balance control model represents a quantitative hypothesis about the organization and function of the system, the model can be used to make predictions that motivate new experiments to test these predictions and thereby test the hypothesis represented by the current model. Failure of the model to account for some aspects of new experimental data should then motivate refinements of the existing model or the consideration of alternative model structures (for example see (Mergner et al. 2002; Mergner 2010) for the description of a model structure that is quite different from the one discussed here). The ongoing cycle of model development, followed by experimental challenges, followed by model refinement simply represents the productive application of the scientific method. The general trend will be for the models to become more complex as they become better able to explain the complex nature of balance control.

However, it is also worth noting that simpler models retain some value. As a specific example, the Fig. 9.5a model does account for the main dynamic characteristics of the stance control system. Parameters determined from a fit of this model to FRFs of individual subjects provide quantitative measures with physiological relevance, such as sensory weights. Tests that quantify the function of the balance control system using a model-based interpretation of stimulus-response behavior could be used clinically to diagnose neurological disorders, track changes over time, or monitor the effectiveness of therapy.

9.4 Investigation of Balance Control During Gait

Of interest to us is whether or not the sensory integration principles identified for stance control also apply to the control of body orientation during gait. If so, then we would expect the mean body orientation during gait would be significantly influenced by environmental conditions such as walking on a sloped surface.

As with our studies of stance control, we want to have an experimental data set that is rich enough to promote the development of models that help us to understand the mechanisms contributing to the control of body orientation and dynamic stability during gait. Our prior use of pseudorandom stimuli and FRF analysis methods to study stance control motivated us to apply similar methods to study gait. The experimental results reported here focus on the control of body orientation in the frontal plane.

In order to apply pseudorandom stimuli during gait, we adopted a stepping-in-place (SiP) protocol as a surrogate for walking gait. The roll motions of the body CoM during SiP (Fig. 9.7a) closely resemble the frontal plane motions of the CoM during forward walking (Brenière 1996; Hof et al. 2005). Specifically, the CoM oscillates right and left with a sinusoidal motion, and the peak lateral displacement of the CoM is typically located medial of the stance foot. The CoP oscillates right and left with plateaus occurring when only 1 ft is on the surface. The CoP shows a ramp trajectory during the double leg support phase as weight is shifted from 1 ft to the other. From analysis of the CoP trajectory, the timing of the gait-cycle events can be measured.

All SiP tests were performed with eyes closed. To maintain an approximately constant location of the subject during SiP on the surface of our balance test device, soft foam guides were taped to the surface in a T-shaped configuration. Subjects were instructed to make small corrections in stepping location when they made contact with the T.

Balance in the frontal plane was perturbed using pseudorandom surface-tilt stimuli (six cycles per test trial, peak-to-peak amplitudes of 0° (control trial), 1°, 2°, and 4°) while subjects performed SiP. Metronome clicks were used to pace the stepping such that subjects performed 38 step cycles in each 48.4-s cycle of the pseudorandom stimulus (i.e., stepping frequency of ~0.8 Hz). Measurements included subject CoM sway angle in the frontal plane, lateral displacement of the CoP, and lateral displacements of right and left heels. The same stimuli were used to evoke frontal-plane sway during stance. Stance trials were performed eyes closed with the feet separated by 8 cm (intermalleolar distance). CoM sway in response the surface-tilt stimulus was analyzed to calculate FRFs from SiP trials and stance trials. Step width and step timing were also measured in order to investigate mechanisms contributing to the control of dynamic balance (Kuo 1999; Hausdorff 2005; Maufroy et al. 2010), but only results related to the control of body orientation are discussed below.

9.4.1 Control of Body Orientation During Gait

Do the principles of sensory integration and sensory reweighting identified for stance control also apply to the control of body orientation during gait? The results from sway measured during eyes closed SiP suggest there are similarities. Figure 9.7b shows one subject's frontal-plane CoM sway during a SiP test while balance was perturbed by a continuous pseudorandom tilt of the surface upon which the subject was stepping. Results are shown for three different stimulus amplitudes

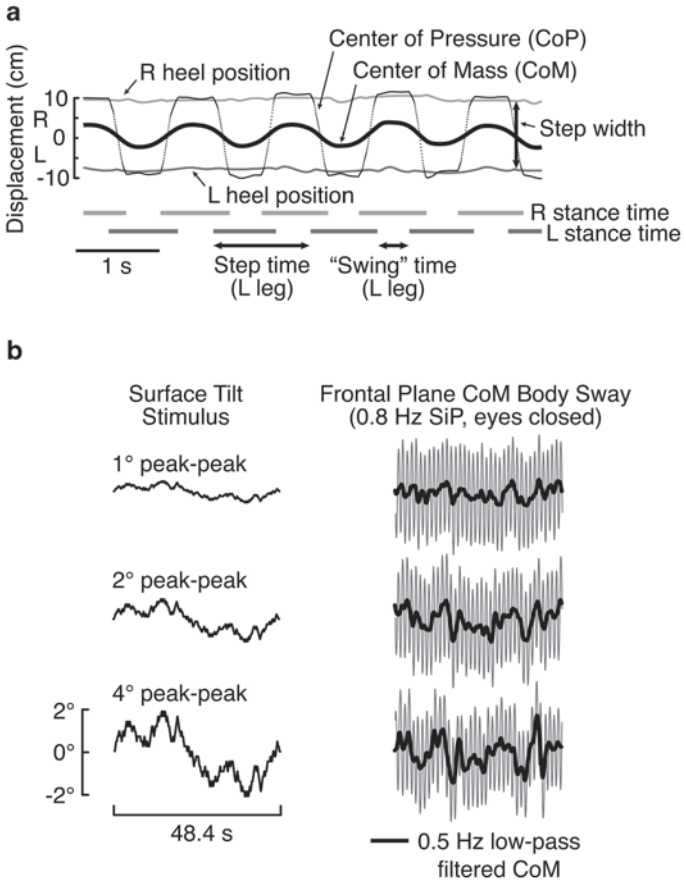

Fig. 9.7 Results from stepping-in-place (*SiP*) experiments. **a** Example data recorded during SiP showing frontal-plane displacements of center-of-pressure (*CoP*), center-of-mass (*CoM*), and *right* and *left* heel position from which step-by-step measures of step width and step timing (stance times and swing times of *right* and *left* legs) were taken. **b** Example CoM sway recorded from an individual subject during eyes-closed SiP on a surface that was rotated according to a pseudorandom waveform at three different amplitudes. CoM sway data, averaged across five cycles of the pseudorandom stimuli, shows that the oscillating pattern of CoM in the frontal plane (*gray* traces) is disturbed by the surface-tilt stimulus. Application of a 0.5 Hz low-pass filter to the CoM eliminates the oscillatory component at the 0.8 Hz SiP frequency and reveals the deviations of the CoM orientation across the stimulus cycle (thick *black* traces)

and the CoM sway data were averaged across the last five cycles of the pseudorandom stimulus. The regularity of oscillations occurring at the 0.8 Hz stepping frequency become more disrupted at larger stimulus amplitudes due to changes in body orientation evoked by the stimulus. The time course of the change in body orientation is made more evident by low-pass filtering (0.5 Hz cutoff frequency) the CoM sway data to remove the 0.8-Hz oscillation at the stepping frequency. The low-pass filtered CoM traces (thick traces) tend to increase with increasing stimulus amplitude and show some resemblance to the time course or the stimulus waveform.

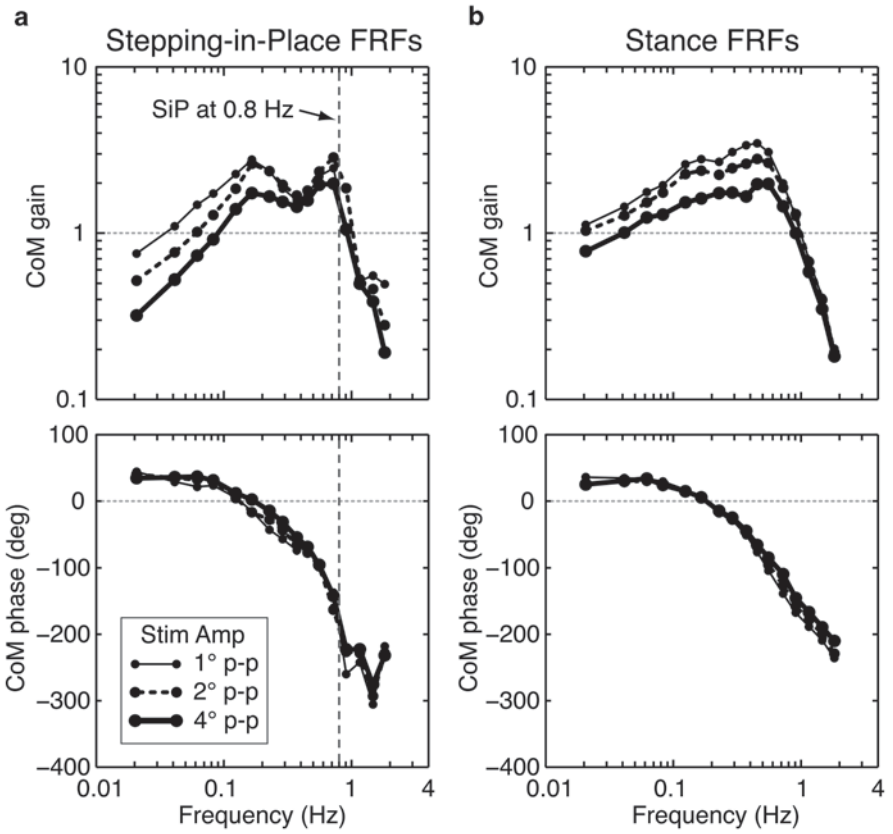

Fig. 9.8 Frequency response functions (*FRFs*) from SiP experiments (**a**) and stance experiments (**b**). Pseudorandom surface-tilt stimuli at three different amplitudes were used to evoke CoM sway in the frontal plane. FRF results were averaged across the data from six subjects with normal sensory function who performed both SiP and stance experiments with eyes closed

FRFs calculated from the CoM sway evoked by surface-tilt stimulation during SiP are shown in Fig. 9.8a. For comparison, FRFs from stance trials of the same subjects are also shown in Fig. 9.8b. Each set of FRFs show results for the three different stimulus amplitudes and the FRFs are average results from six young adult subjects with normal sensory function. There were similarities and differences between FRFs from stance and SiP trials. Both showed the largest gains in the mid-frequency region, decreasing gains with decreasing frequencies below about 0.1 Hz, and decreasing gains with increasing frequencies above about 0.8 Hz. Mid-frequencies gains were greater than unity for both SiP and stance indicating the high sensitivity to surface-tilt perturbations in this mid-frequency range. Results from SiP and stance both showed decreasing FRF gains with increasing stimulus amplitude. For the SiP FRFs, this gain decrease with increasing amplitude was evident at frequencies below about 0.2 Hz while for stance FRFs, the amplitude-dependent

gain decrease was evident at frequencies below about 0.8 Hz. Both SiP and stance FRFs showed phase leads at frequencies below about 0.2 Hz, and increasing phase lags at higher frequencies. SiP and stance phase data was minimally influenced by stimulus amplitude.

Differences between SiP and stance FRFs relate to the detailed shapes of the gain curves. The SiP gain curves show a notched decrease in gain at about 0.4 Hz and a peak near the stepping frequency while the stance gain curves are more uniform in this frequency region. It is perhaps notable that a previous study, that perturbed balance during treadmill walking using a sinusoidal visual stimulus at various frequencies, observed a similar enhancement of lateral sway amplitude when the stimulus frequency was close to the walking frequency (Kay and Warren 2001).

To the extent that we are confident that an amplitude-dependent change in FRF gains in the absence of phase changes is indicative of a sensory reweighting phenomenon, the pattern of amplitude-dependent changes seen in the SiP FRFs implies that the same or a very similar sensory reweighting phenomenon is contributing to the regulation of body orientation during SiP. Because the frontal-plane body motion during SiP and actual walking gait are similar, we anticipate that the balance mechanisms regulating the control of quiet stance are also influencing frontal-plane balance control during walking. As discussed previously, the balance mechanisms regulating body orientation during stance do a relatively poor job of maintaining an upright body orientation in conditions where the surface is not level or the visual system is not providing accurate orientation information. Therefore when walking on a tilted surface, for example, the mechanisms that control body orientation will evoke a leaning posture, and this leaning posture will impose a mechanical asymmetry that would be expected to complicate the task of maintaining dynamic stability during gait.

The FRF gain values at the lowest frequencies are notably smaller for the SiP trials than the stance trials, particularly in the results from the largest stimulus amplitude where the SiP gains are about half the value of the stance trials. The gain decrease and phase advance at lower frequencies are consistent with a torque feedback mechanism contributing to the control of body orientation at these lower frequencies. The lower low-frequency gains during SiP compared to stance suggest that this mechanism made a stronger contribution to orientation control during SiP. Assuming that SiP results apply to actual walking, a low FRF gain at low frequencies predicts that the mean body orientation would be close to zero (i.e., vertical) if a subject were walking for an extended period of time across a surface with a constant slope. However, if the slope was changing, as it would be on uneven terrain, the mean body orientation will be affected to a much greater extent and thus have a greater impact on the task of maintaining both static and dynamic stability, thus perhaps increasing the likelihood of falling.

Acknowledgements All experiments were performed according to protocols approved by the IRB of Oregon Health & Science University. Work was supported by NIH grants R01AG17960 and R01DC010779.

References

Ahn J, Hogan N (2013) Long-range correlations in stride intervals may emerge from non-chaotic walking dynamics. PLoS One 8:e73239

Alexandrov AV, Frolov AA, Horak FB, Carlson-Kuhta P, Park S (2005) Feedback equilibrium control during human standing. Biol Cybern 93:309–322

Angelaki DE, McHenry MQ, Dickman JD, Newlands SD, Hess BJ (1999) Computation of inertial motion: neural strategies to resolve ambiguous otolith information. J Neurosci 19:316–327

Angelaki DE, Shaikh AG, Green AM, Dickman JD (2004) Neurons compute internal models of the physical laws of motion. Nature 430:560–564

Bauby CE, Kuo AD (2000) Active control of lateral balance in human walking. J Biomech 33:1433–1440

Bendat JS, Piersol AG (2000) Random data: analysis and measurement procedures, 3rd edn. Wiley, New York

Boonstra TA, Schouten AC, van der Kooij H (2013) Identification of the contribution of the ankle and hip joints to multi-segmental balance control. J Neuroeng Rehabil 10:23

Bosco G, Poppele RE, Eian J (2000) Reference frames for spinal proprioception: limb endpoint based or joint-level based? J Neurophysiol 83:2931–2945

Brenière Y (1996) Why we walk the way we do. J Mot Behav 28:291–298

Casabona A, Stella Valle M, Bosco G, Perciavalle V (2004) Cerebellar encoding of limb position. Cerebellum 3:172–177

Cenciarini M, Peterka RJ (2006) Stimulus-dependent changes in the vestibular contribution to human postural control. J Neurophysiol 95:2733–2750

Davies WDT (1970) System identification for self-adaptive control. Wiley-Interscience, London

Dean JC, Alexander NB, Kuo AD (2007) The effect of lateral stabilization on walking in young and old adults. IEEE Trans Biomed Eng 54:1919–1926

Dingwell JB, Cusumano JP (2000) Nonlinear time series analysis of normal and pathological human walking. Chaos 10:848–863

Duysens J, Clarac F, Cruse H (2000) Load-regulating mechanisms in gait and posture: comparative aspects. Physiol Rev 80:83–133

Fujisawa N, Masuda T, Inaoka H, Fukuoka Y, Ishida A, Minamitani H (2005) Human standing posture control system depending on adopted strategies. Med Biol Eng Comput 43:107–114

Goodworth AD, Peterka RJ (2009) Contribution of sensorimotor integration to spinal stabilization in humans. J Neurophysiol 102:496–512

Goodworth AD, Peterka RJ (2010a) Influence of bilateral vestibular loss on spinal stabilization in humans. J Neurophysiol 103:1978–1987

Goodworth AD, Peterka RJ (2010b) Influence of stance width on frontal plane postural dynamics and coordination in human balance control. J Neurophysiol 104:1103–1118

Goodworth AD, Peterka RJ (2012) Sensorimotor integration for multisegmental frontal plane balance control in humans. J Neurophysiol 107:12–28

Hausdorff JM (2005) Gait variability: methods, modeling and meaning. J Neuroeng Rehabil 2:19

Hettich G, Assländer L, Gollhofer A, Mergner T (2014) Human hip-ankle coordination emerging from multisensory feedback control. Human Movement Science 37:123–146

Hof AL, Gazendam MGJ, Sinke WE (2005) The condition for dynamic stability. J Biomech 38:1–8

Horak FB, Macpherson JM (1996) Postural orientation and equilibrium. In: Rowell LB, Shepherd JT (eds) Handbook of physiology: section 12: exercise: regulation and integration of multiple systems. Oxford University Press, New York, pp 255–292

Johansson R, Magnusson M, Akesson M (1988) Identification of human postural dynamics. IEEE Trans Biomed Eng 35:858–869

Kay BA, Warren WH (2001) Coupling of posture and gait: mode locking and parametric excitation. Biol Cybern 85:89–106

Kiemel T, Elahi AJ, Jeka JJ (2008) Identification of the plant for upright stance in humans: multiple movement patterns from a single neural strategy. J Neurophysiol 100:3394–3406.

Kim S, Atkeson CG, Park S (2012) Perturbation-dependent selection of postural feedback gain and its scaling. J Biomech 45:1379–1386
Kuo AD (1999) Stabilization of lateral motion in passive dynamic walking. Int J Robot Res 18:917–930
Li Y, Levine WS, Loeb GE (2012) A two-joint human posture control model with realistic neural delays. IEEE Trans Neural Syst Rehabil Eng 20:738–748
Loram ID, Maganaris CN, Lakie M (2005) Non-invasive tracking of contractile length. J Appl Physiol 100:1311–1323
Markert G, Büttner U, Straube A, Boyle R (1988) Neuronal activity in the flocculus of the alert monkey during sinusoidal optokinetic stimulation. Exp Brain Res 70:134–144
Maufroy C, Kimura H, Takase K (2010) Integration of posture and rhythmic motion controls in quadrupedal dynamic walking using phase modulations based on leg loading/unloading. Auton Robot 28:331–333
McMahon TA (1984) Muscles, reflexes, and locomotion. Princeton University Press, Princeton
Merfeld DM, Zupan L, Peterka RJ (1999) Humans use internal models to estimate gravity and linear acceleration. Nature 398:615–618
Mergner T (2004) Meta level concept versus classic reflex concept for the control of posture and movement. Arch Ital Biol 142:175–198
Mergner T (2010) A neurological view on reactive human stance control. Anu Rev Control 34:177–198
Mergner T, Maurer C, Peterka RJ (2002) Sensory contributions to the control of stance: a posture control model. Adv Exp Med Biol 508:147–152
Mummolo C, Mangialardi L, Kim JH (2013) Quantifying dynamic characteristics of human walking for comprehensive gait cycle. J Biomech Eng 135:91006
Nashner LM (1981) Analysis of stance posture in humans. In: Towe AL, Luschei ES (eds) Handbook of behavioral neurobiology, vol 5. Plenum Publishing Corporation, New York, pp 527–565
Otnes RK, Enochson L (1972) Digital time series analysis. Wiley, New York
Park S, Horak FB, Kuo AD (2004) Postural feedback responses scale with biomechanical constraints in human standing. Exp Brain Res 154:417–127
Pasma JH, Boonstra TA, Campfens SF, Schouten AC, van der Kooij H (2012) Sensory reweighting of proprioceptive information on the left and right leg during human balance control. J Neurophysiol 108:1138–1148
Peterka RJ (2002) Sensorimotor integration in human postural control. J Neurophysiol 88:1097–1118
Peterka RJ (2003) Simplifying the complexities of maintaining balance. IEEE Eng Med Biol Mag 22:63–68
Peterka RJ, Benolken MS (1995) Role of somatosensory and vestibular cues in attenuating visually induced human postural sway. Exp Brain Res 105:101–110
Peterka RJ, Black FO, Schoenhoff MB (1990) Age-related changes in human vestibulo-ocular and optokinetic reflexes: Pseudorandom rotation tests. J Vestib Res 1:67–71
Peterka RJ, Gianna-Poulin CC, Zupan LH, Merfeld DM (2004) Origin of orientation-dependent asymmetries in vestibulo-ocular reflexes evoked by caloric stimulation. J Neurophysiol 92:2333–2345
Pintelon R, Schoukens J (2012) System identification: a frequency domain approach. IEEE Press, New York
Prochazka A, Gillard D, Bennett DJ (1997) Positive force feedback control of muscles. J Neurophysiol 77:3226–3236
Terry K, Sinitski EH, Dingwell JB, Wilken JM (2012) Amplitude effects of medio-lateral mechanical and visual perturbations. J Biomech 45:1979–1986
van der Kooij H, Peterka RJ (2011) Non-linear stimulus-response behavior of the human stance control system is predicted by optimization of a system with sensory and motor noise. J Comput Neurosci 30:759–778

van der Kooij H, Jacobs R, Koopman B, Grootenboer H (1999) A multisensory integration model of human stance control. Biol Cybern 80:299–308

Winter DA (1995) Human balance and posture control during standing and walking. Gait Posture 3:193–214

Zupan LH, Peterka RJ, Merfeld DM (2000) Neural processing of gravito-inertial cues in humans. I. Influence of the semicircular canals following post-rotatory tilt. J Neurophysiol 84:2001–2015